ISSN 1027-4510, Journal of Surface Investigation. X-ray, Synchrotron and Neutron Techniques, 2014, Vol. 8, No. 1, pp. 84–92. © Pleiades Publishing, Ltd., 2014.
Original Russian Text © R.M. Khusnutdinoff, A.V. Mokshin, I.I. Khadeev, 2014, published in Poverkhnost'. Rentgenovskie, Sinkhrotronnye i Neitronnye Issledovaniya, 2014, No. 1, pp. 90–98.

Microscopic Collective Dynamics of Atoms in the Amorphous Metallic Alloy $Ni_{33}Zr_{67}$

R. M. Khusnutdinoff, A. V. Mokshin, and I. I. Khadeev

Kazan Federal University, Kazan, 420008 Russia

Received April 15, 2013

Abstract—The structural properties and microscopic collective dynamics of atoms in the amorphous metallic alloy $Ni_{33}Zr_{67}$ are studied using molecular dynamics simulations with a pair-additive model potential. The calculated equilibrium structural and dynamic characteristics are compared with experimental data on neutron diffraction and inelastic X-ray scattering. Theoretical analysis of the structural relaxation of microscopic density fluctuations for amorphous metallic alloys is performed within the Lee's recurrent relation approach. The results of theoretical calculations for the intensity of scattering $I(k, \omega)$ for the amorphous metallic alloy $Ni_{33}Zr_{67}$ are in good agreement with the results of computer simulation and experimental inelastic X-ray scattering data. The low-frequency excitations observed in the longitudinal current spectra are related to the vibrational motions of individual atom clusters, which include Ni and Zr atoms.

DOI: 10.1134/S1027451014010133

INTRODUCTION

Amorphous metallic alloys (AMA) are prospective materials, which attract the special interest of scientists and technologists by their unique physical-chemical and mechanical properties [1–8]. For example, amorphous alloys containing transition metals (Fe, Co, Ni) as the main component have a high tensile-strength limit, which exceeds by more than two times the characteristics of their crystalline counterparts. Some of these amorphous alloys also have high corrosion stability, and excellent magnetic and electric properties. All these properties of AMA are related with the presence of local structural disorder [5, 6].

The amorphous metallic alloys NiZr are characterized by the following features [9]: (i) the structure of the alloys has pronounced short-range topological order which strongly affects the dispersion curve in the amorphous state; (ii) they have a large coherent cross section of neutron scattering which is an important characteristic at comparison the simulation and theoretical results with of experimental data. At present the alloy $Zr_{41.2}Ti_{13.8}Cu_{12.5}Ni_{10.0}Be_{22.5}$ (Vitreloy 1), which can form a bulk amorphous phase at a cooling rate of ~1 K/s, is widely known [10]. This and other features stimulate a large number of experimental and theoretical studies [5–10].

In Ref. [11] the effect of the concentration dependence of Ni_xZr_{100-x} alloys (x = 5, 10, 16.7, 33.3, 0.5, 66.7, 83.3, 90.0, 95.0) on the processes of crystallization was studied via computer simulations. It was shown that the highest degree of crystallization corresponds to the alloy with a high nickel content, i.e., $Ni_{66.7}Zr_{33.3}$. It was established that crystallization in alloys is due to an increase in the number of icosahedral quasicrystalline clusters.

The dynamic properties of the $Ni_{33}Zr_{67}$ alloy in the amorphous and crystalline phases were studied in Ref. [12] by means of inelastic neutron scattering technique. By comparison of spectra of the dynamic structure factor $S(k, \omega)$ for amorphous and for crystalline phases, the authors concluded that the propagation of collective excitations in metallic glass $Ni_{33}Zr_{67}$ is due to "optical" excitations corresponding to the crystalline phase. The authors supposed that three optical modes in the $Ni_{33}Zr_{67}$ crystal can also exist in the amorphous phase on a short timescale. However, subsequent experimental studies [13] did not confirm this hypothesis about the nature of collective excitations in amorphous metallic alloys.

In this work the microscopic dynamic processes in the amorphous metallic alloy $Ni_{33}Zr_{67}$ are studied in order to clarify the mechanism of the origin and propagation of collective excitations in the terahertz frequency region.

THEORY OF STRUCTURAL RELAXATION

The differential scattering cross-section in experiments on inelastic X-ray scattering is proportional to the so-called dynamic structure factor $S(k, \omega)$, which is a Fourier transform of the coherent scattering function [14–17]

$$F(k,t) = \left\langle \delta\rho_k^*(0)\delta\rho_k(t) \right\rangle. \quad (1)$$

Here, the angular brackets denote averaging over the equilibrium ensemble, and the quantity

$$\delta\rho_k(t) = \frac{1}{\sqrt{N}}\sum_{j=1}^{N}\exp\left(-i\mathbf{k}\mathbf{r}_j(t)\right) \quad (2)$$

is the local density fluctuation; N is the number of atoms forming the system; $\mathbf{r}_j(t)$ is the radius-vector for the jth atom at the moment of time t and $\mathbf{k}$ is the wave vector.

The time evolution of the density fluctuation is determined by the Heisenberg equation [18]:

$$\frac{d\delta\rho_k(t)}{dt} = i\hat{L}\delta\rho_k(t), \quad (3)$$

where $\hat{L}$ is the self-consistent Liouville operator. According to the Lee's recurrent relation approach [19–23], the $\delta\rho_k(t)$ value can formally be presented in the form of a vector in abstract d-dimensional space [17]:

$$\delta\rho_k(t) = \sum_{m=0}^{d-1} a_m(k,t)f_m(k). \quad (4)$$

here $f_0(k), f_1(k), \ldots, f_{d-1}(k)$ is a complete set of "basis vectors" forming the space S. "Vectors" $f_0(k), f_1(k), \ldots, f_{d-1}(k)$ satisfy the condition $(f_m(k), f_{m'}(k)) = 0$ at $m \neq m'$ and are related by the following recurrence relation (RR-I):

$$\begin{gathered} f_{m+1}(k) = i\hat{L}f_m(k) + \Delta_m(k)f_{m-1}(k), \quad m \geq 0, \\ \Delta_m(k) = \frac{\left(f_m(k), f_m(k)\right)}{\left(f_{m-1}(k), f_{m-1}(k)\right)}, \\ f_{-1}(k) = 0, \quad \Delta_0(k) \equiv 0. \end{gathered} \quad (5)$$

Here, the brackets (..,..) denote the Kubo scalar product [24]; $\Delta_m(k)$ is the recurrant or mth-order relaxation parameter; $a_m(k,t)$ are the so-called basis-functions [$F(k, t) = a_0(k, t)$], which are related by the second recurrence relation (RR-II) [19]:

$$\begin{gathered} \Delta_{m+1}(k)a_{m+1}(k,t) = -\frac{da_m(k,t)}{dt} + a_{m-1}(k,t), \\ 0 \leq m \leq d-1. \end{gathered} \quad (6)$$

Thus, a set of recurrence relations (5) and (6) leads to the time evolution of the dynamic variable $\delta\rho_k(t)$, which appears in the space formed by the orthogonal basis vectors $f_m(k), f_{m+1}(k), \ldots$.

Applying the Laplace transformation to the last equation, it is possible to obtain a relation:

$$\tilde{a}_m(k,z) = \left[z + \Delta_{m+1}(k)\tilde{a}_{m+1}(k,z)\right]^{-1}, \quad (7)$$

which can be presented in the form of the continued fraction [1]

$$\tilde{a}_0(k,z) = \cfrac{1}{z + \cfrac{\Delta_1(k)}{z + \cfrac{\Delta_2(k)}{z + \cfrac{\Delta_3(k)}{z + \ddots}}}}, \quad (8)$$

The parameters $\Delta_{m+1}(k)$ can be expressed in terms of the normalized frequency moments of the dynamic structure factor $S(k, \omega)$ [1]:

$$\omega^{(m)}(k) = \frac{\int_{-\infty}^{\infty}\omega^m S(k,\omega)d\omega}{\int_{-\infty}^{\infty}S(k,\omega)d\omega}, \quad (9)$$

when $S(k, \omega)$ is related to the Fourier transform $a_0(k, t)$ by the relation

$$S(k,\omega) = \frac{S(k)}{2\pi}\int_{-\infty}^{\infty}\exp\left(i\omega t\right)a_0(k,t)dt. \quad (10)$$

By solving Eqs. (5) and (9), it is possible to find expressions relating the frequency moments of the dynamic structure factor with the relaxation parameters [25]:

$$\begin{gathered} \omega^{(2)}(k) = \Delta_1(k), \\ \omega^{(4)}(k) = \Delta_1^2(k) + \Delta_1(k)\Delta_2(k), \\ \omega^{(6)}(k) = \Delta_1(k)\left[\Delta_1(k) + \Delta_2(k)\right]^2 + \Delta_1(k)\Delta_2(k)\Delta_3(k), \\ \omega^{(8)}(k) = \Delta_1(k)\left\{\left[\Delta_1(k) + \Delta_2(k)\right]^3 + 2\Delta_2(k)\Delta_3(k)\right. \\ \left.\times\left[\Delta_1(k) + \Delta_2(k)\right] + \Delta_2(k)\Delta_3^2(k)\right\} \\ + \Delta_1(k)\Delta_2(k)\Delta_3(k)\Delta_4(k), \\ \ldots\ldots\ldots \end{gathered} \quad (11)$$

Using Eqs. (5) and (9), one can find the expressions for the parameters $\Delta_n(k)$ [17]:

$$\begin{gathered} \Delta_1(k) = \frac{k_B T}{m}\frac{k^2}{S(k)}, \\ \Delta_2(k) = \frac{k_B T}{m}k^2\left(3 - \frac{1}{S(k)}\right) \\ + \frac{n}{m}\int\nabla_l^2 U(r)\left[1 - \cos\left(kr\right)\right]g(r)dr, \\ \Delta_3(k) = \frac{1}{\Delta_2(k)}\left\{15\left(\frac{k_B T}{m}k^2\right) + F(k)\right\} \\ - \frac{1}{\Delta_2(k)}\left[\Delta_1(k) + \Delta_2(k)\right]^2. \end{gathered} \quad (12)$$

Here, n denotes the number density of the system, $S(k)$ is the static structure factor, $g(r)$ is the radial particle-distribution function, $U(r)$ is the interatomic interaction potential. The index l denotes the component

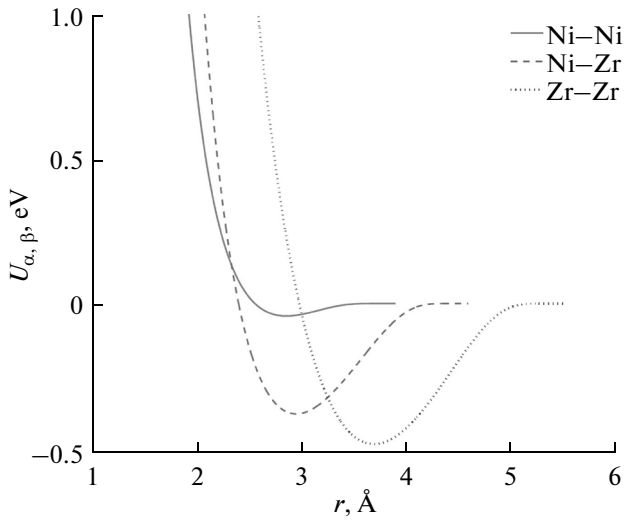

Fig. 1. Interaction potential between different components of the alloy $Ni_{33}Zr_{67}$.

parallel to vector **k**, quantity $F(k)$ denotes the combination of integral expressions containing the interparticle potential as well as two- and three-particle distribution functions. In the general case, the $\Delta_n(k)$ parameters of higher orders n also contain distribution functions of n, $(n-1)$, ... and $n=2$ orders. Consequently, if the studied system is characterized by strongly expressed potential interactions, the problem of finding the time evolution of the local density fluctuation of the number of particles is reduced to decoupling the chain equations for the n-particle distribution functions [26]. It was empirically established in Ref. [27] that the high-order relaxation parameters satisfy to the condition $[\Delta_4(k) \approx \Delta_5(k) \approx \Delta_6(k)]$, which makes it possible to obtain an expression for the dynamic structure factor from Eqs. (8) and (10) in the form:

$$S(k,\omega) = \frac{S(k)}{2\pi}\Delta_1(k)\Delta_2(k)\Delta_3(k)\sqrt{4\Delta_4(k)-\omega^2} \times \left\{\Delta_1^2(k)\Delta_3^2(k) + \omega^2\left[-2\Delta_1(k)\Delta_3^2(k) + \Delta_1^2(k)\Delta_4(k) - \Delta_1^2(k)\Delta_3(k) + 2\Delta_1(k)\Delta_2(k)\Delta_4(k) - \Delta_1(k)\Delta_2(k)\Delta_3(k) + \Delta_2^2(k)\Delta_4(k)\right] + \omega^4\left[\Delta_3^2(k) - 2\Delta_1(k)\Delta_4(k) + 2\Delta_1(k)\Delta_3(k) - 2\Delta_2(k)\Delta_4(k) + \Delta_2(k)\Delta_3(k)\right] + \omega^6\left[\Delta_4(k) - \Delta_3(k)\right]\right\}^{-1}. \quad (13)$$

SIMULATION DETAILS

Computer molecular dynamics simulations (MD) of the amorphous metallic alloy $Ni_{33}Zr_{67}$ was performed at the temperature $T = 300$ K. The considered system was consisted of $N = 10\,976$ particles ($N_{Ni} = 3535$ and $N_{Zr} = 7441$), where the number density is $n = 0.0427$ Å^{-3} (mass density = 5.7255 g/cm^3). The interaction between atoms was implemented using the interatomic interaction potential proposed in [28]:

$$U_{\alpha,\beta}(r) = A_{\alpha,\beta}\left[\frac{1}{\left(\zeta_{\alpha,\beta}r - a_{\alpha,\beta}\right)^n} - 1\right]\exp\left(\frac{1}{\zeta_{\alpha,\beta}r - b_{\alpha,\beta}}\right), \quad \left(r < \frac{a_{\alpha,\beta}}{\zeta_{\alpha,\beta}}\right). \quad (14)$$

Here $\alpha,\beta \in \{Ni, Zr\}$ and $A_{\alpha,\beta}$, $\zeta_{\alpha,\beta}$, $a_{\alpha,\beta}$, $b_{\alpha,\beta}$ are parameters of the potential from Ref. [28]. The interaction potential between different components of the mixture is shown in Fig. 1.

The simulation was performed in the isothermal–isobaric ensemble (NpT). To maintain the system in thermal equilibrium, the Berendsen's thermostat and barostat with the coupling parameter $\tau = 10^{-14}$ s were used [29]. Avoiding crystallization by fast cooling, the system from the stable liquid state ($T = 3000$ K) was transferred into the amorphous metastable state ($T = 300$ K). The system was cooled in the isoenthalpy–isobaric ensemble (NpH) at a cooling rate of $dT/dt = 10^{13}$ K/s. The equations of particle motion were integrated using the velocity Verlet integration algorithm with a time step of 10^{-15} s.

SIMULATION RESULTS

Structural Properties of the Amorphous Metallic Alloy $Ni_{33}Zr_{67}$

The structural features of the metallic alloy were analyzed on the basis of calculation of the partial radial distribution function of particles in the system (Fig. 2) [30]:

$$g_{\alpha,\beta}(r) = \frac{V}{N_\alpha N_\beta}\left\langle\sum_{i=1}^{\alpha}\sum_{j=1}^{\beta}\delta\left(r - r_{ij}\right)\right\rangle, \quad \alpha,\beta \in \{\mathrm{Ni},\mathrm{Zr}\}, \quad (15)$$

and the static structure factor $S(k)$. The partial components of the static structure factor were calculated on the basis of a Fourier transform of the radial distribution function of atoms [31]:

$$S_{\alpha,\beta}(k) = \delta_{\alpha,\beta} + 4\pi n\int_0^\infty r^2\left[g_{\alpha,\beta}(r) - 1\right]\frac{\sin(kr)}{kr}dr. \quad (16)$$

The total static structure factor was found via spatial Fourier transform of the total radial distribution function of the particles, which, in turn, was calculated using the following relation [32]

$$g(r) = \frac{1}{\left(c_1 b_1 + c_2 b_2\right)}\sum_{\alpha,\beta}^{2}\sqrt{c_\alpha c_\beta}f_\alpha f_\beta g_{\alpha,\beta}(r), \quad \alpha,\beta \in \{\mathrm{Ni},\mathrm{Zr}\}, \quad (17)$$

where c is the concentration of particles, f is the scattering length (in the case of neutron scattering). Figure 3 shows the partial components and the total static structure factor obtained on the basis of computer

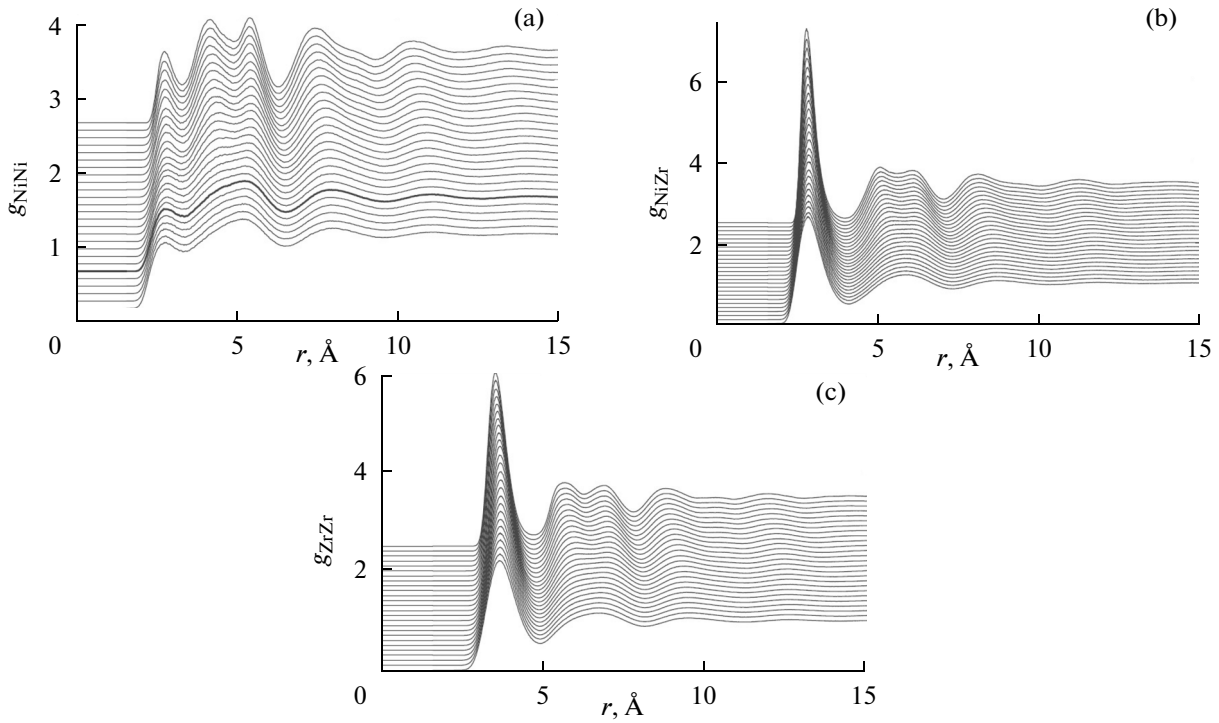

Fig. 2. Temperature dependence of the partial radial-distribution function of particles of the $Ni_{33}Zr_{67}$ system for: (a) pairs of Ni–Ni atoms; (b) components of the Ni–Zr system and (c) Zr–Zr atoms.

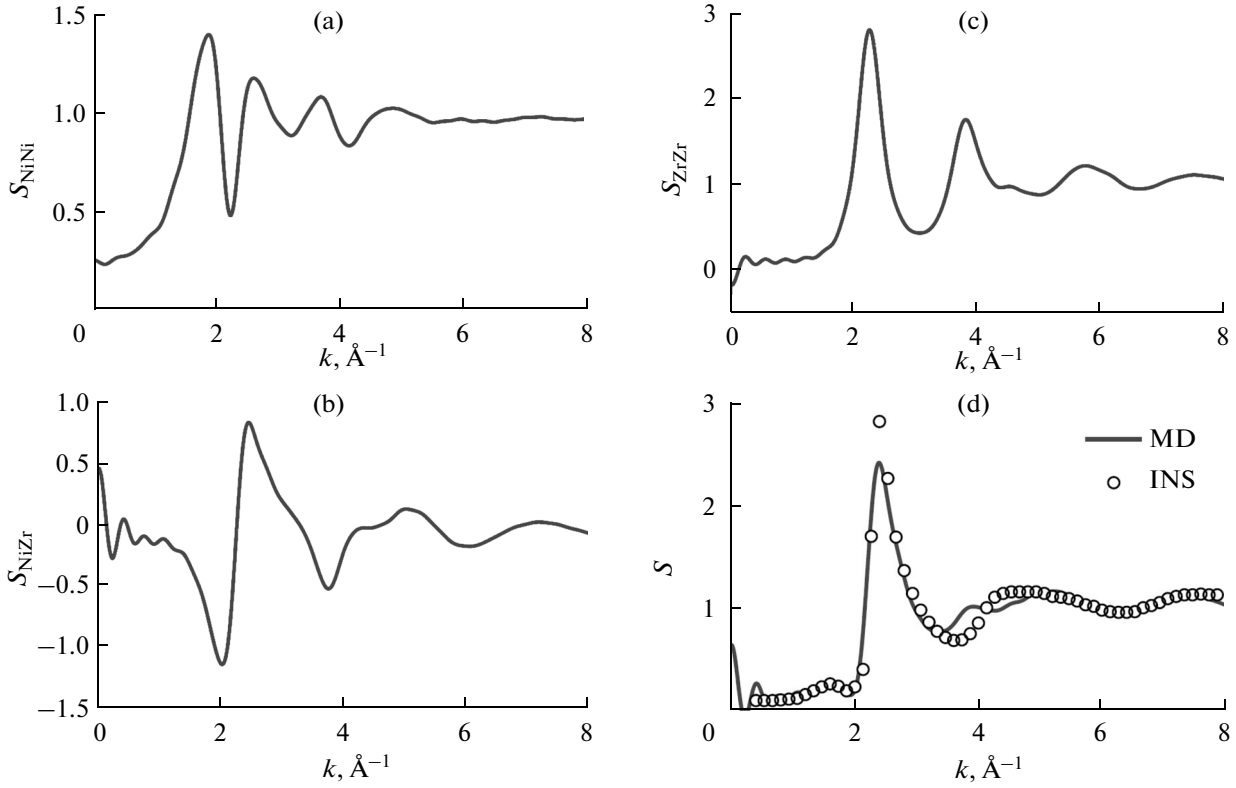

Fig. 3. Static structure factor of the alloy $Ni_{33}Zr_{67}$ at the temperature of $T = 300$ K: the solid line presents the results of the molecular dynamics simulation; the marks denote experimental data of neutron diffraction [33]. Partial components of the static structure factor for a pair of atoms: (a) Ni–Ni, (b) Ni–Zr, (c) Zr–Zr and (d) total static structure factor.

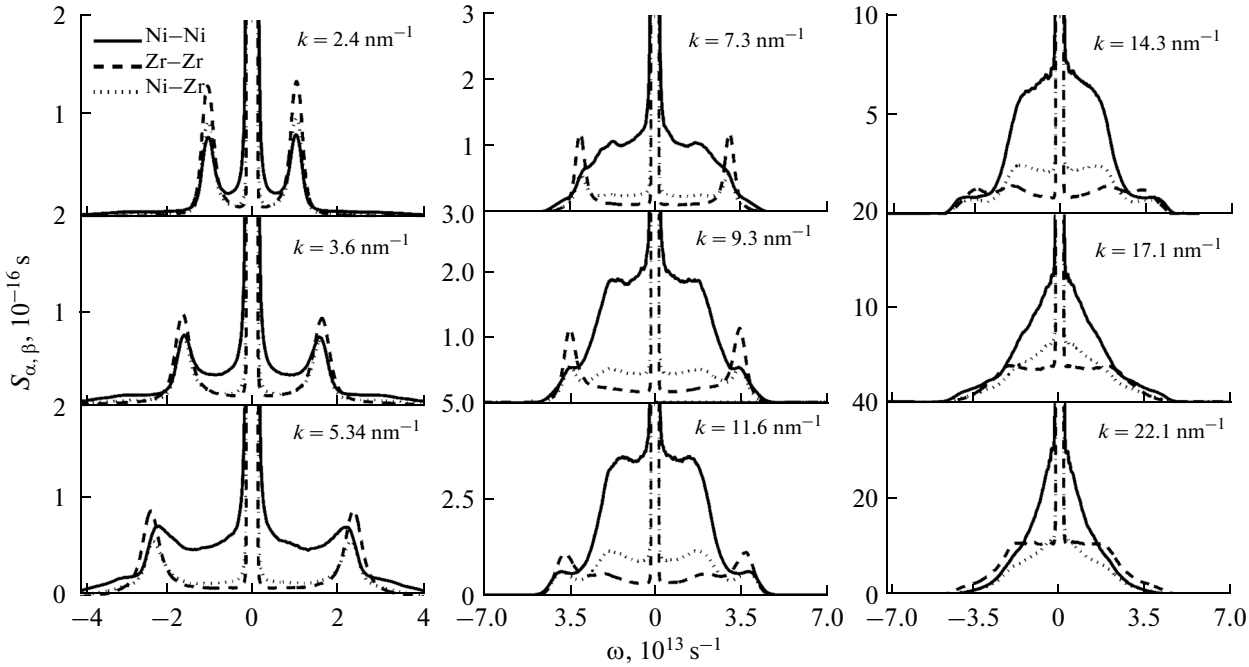

Fig. 4. Partial components of the dynamic structural factor of the alloy $Ni_{33}Zr_{67}$ at a temperature of $T = 300$ K obtained on the basis of molecular dynamics simulation data.

simulation in comparison with the experimental data of neutron diffraction [33]. It is seen from the figure that the simulation results are in good agreement with the experimental data, and as a whole correctly reproduce the experimental $S(k)$.

Dynamic Structure Factor AMA $Ni_{33}Zr_{67}$

The dynamic structure factor $S(k,\omega)$ for the case of binary mixtures [17] is determined by the relation

$$S(k,\omega) = \sum_{i,j=1}^{2} \sqrt{c_1 c_2}\, \frac{f_i(k) f_j(k)}{\left\langle f^2(k) \right\rangle} S_{\alpha,\beta}(k,\omega), \qquad (18)$$

where partial components of the dynamic structure factor have the form [34]:

$$S_{\alpha,\beta}(k,\omega) = \frac{1}{t_M} \left| \int_0^{t_M} \delta\rho_\alpha(k,t)\delta\rho_\beta(k,t) \exp\left(2i\omega t\right) dt \right|; \qquad (19)$$

c_α is the concentration of the atomic type $\alpha \in \{\text{Ni, Zr}\}$, f_α is the atomic form-factor, t_M is the time scale of observation for the variable $\delta\rho_\alpha(k,t)$. The partial components of the dynamic structure factor for the amorphous metallic alloy $Ni_{33}Zr_{67}$ at the temperature $T =$ 300 K for a wide range of wavenumbers is shown in Fig. 4. It is seen from the figure that, in the region of low wavenumber values, the spectra $S_{\alpha,\beta}(k, \omega)$ have a pronounced three-peak structure (the so-called Brillouin triplet [25]), which disappears with increasing k values.

The intensity of inelastic X-ray scattering $I(k, \omega)$ of the binary mixture is connected with the dynamic structure factor $S(k, \omega)$ by the following relation [35]:

$$I(k,\omega) = E(k) \int R(k, \omega - \omega') S_q(k,\omega') d\omega',$$
$$S_q(k,\omega) = \frac{\hbar\beta\omega}{1 - \exp\left(-\hbar\beta\omega\right)} S(k,\omega). \qquad (20)$$

Here $S_q(k, \omega)$ is the quantum dynamic structure factor, $\beta = 1/(k_B T)$ is the inverse temperature, $E(k)$ is the normalization factor, and $R(k, \omega)$ is the experimental resolution function:

$$R(k,\omega) = \frac{1}{\sqrt{\pi}\omega_0(k)} \exp\left(-\omega_2 \big/ \omega_0(k)^2\right), \qquad (21)$$

satisfies the condition of normalization

$$\int_{-\infty}^{\infty} R(k,\omega) d\omega = 1. \qquad (22)$$

A comparison of the results of simulation for the intensity of scattering $I(k, \omega)$ with the experimental data on inelastic X-ray scattering [13] is given in Fig. 5. It is seen in the figure that the simulation results correctly reproduce the low-frequency and high-frequency features of the intensity of inelastic X-ray scattering in a wide range of wavenumber values. However, the simulation results do not show low-frequency excitations in the spectra $I(k, \omega)$ at values $k = 9$–11.4 nm^{-1} observed experimentally.

The results of theoretical calculations for the scattering intensity spectra $I(k, \omega)$ by Eq. (13) are pre-

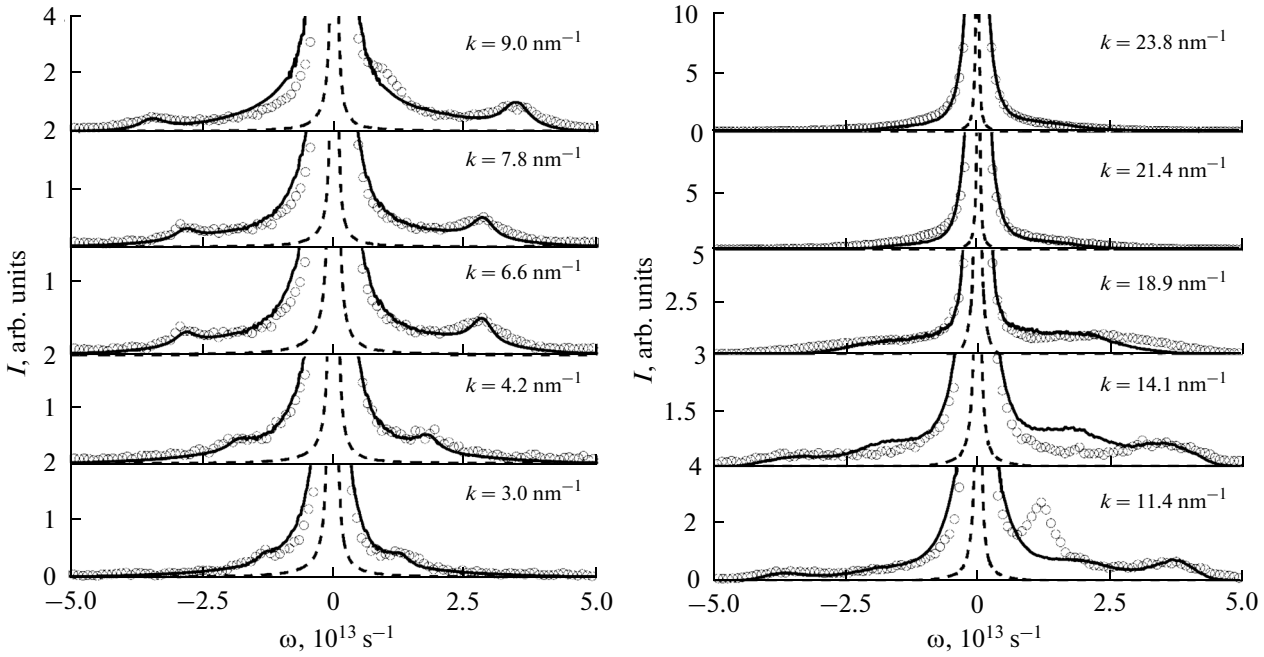

Fig. 5. Intensity of scattering for the amorphous metallic alloy $Ni_{33}Zr_{67}$ at a temperature of $T = 300$ K. The solid line presents the simulation results taking into account the detailed balance condition (20) and the experimental resolution function (21); (○) denote experimental data on inelastic X-ray scattering [13]. The dotted line shows the experimental resolution function.

sented in Fig. 6, where the detailed balance condition (20) and the experimental resolution function (21) taken into account [13]. The values of the first relaxation parameter Δ_1 were calculated exactly on the basis of the molecular-dynamics simulation data using Eqs. (12). The values of parameters $\Delta_2(k)$, $\Delta_3(k)$, and $\Delta_4(k)$ were obtained from the best correspondence between the theory and experimental data. It is seen from the figure, that this theory for the structural relaxation of the density fluctuation of atoms in an amorphous metallic alloy makes it possible to reproduce the complicated form of the scattering intensity spectra $I(k, \omega)$.

The Longitudinal Current Spectra and Dispersion of the Sound Velocity

The dispersion of the sound velocity $\omega_c(k)$, which is directly associated with the position of the high-frequency peak in $S(k, \omega)$, was analyzed on the basis of calculation of the longitudinal current spectra $C_L(k, \omega)$ [36]. This value can be found from the dynamic structure factor $S(k, \omega)$ as:

$$C_L(k,\omega) = \frac{\omega^2}{k^2} S(k,\omega). \qquad (23)$$

Figure 7 shows the partial components of the longitudinal current spectra $C_L(k, \omega)$ at the temperature $T = 300$ K and at different wavenumber values. It is seen from the figure, that an additional low-frequency vibrational mode at $\omega_l(k) \approx 20$ THz appears in the spectrum $C_L(k, \omega)$ with an increase of the wavenumber value. It should be noted that the presence of two inelastic vibrational excitations in the longitudinal current spectra $C_L(k, \omega)$ was observed by Egelstaff et al. [37] as early as in 1968 in experiments on neutron diffraction in liquid lead [38,39]. According to the conclusions [37], the low-frequency branch was explained by the propagation of transverse collective excitations, and the high-frequency branch was related to longitudinal collective excitations in liquid lead. However, later the authors abandoned such interpretation of their own results by relating the appearance of the low-frequency branch to manifestation of the effects of multiple scattering in the experiment.

In Ref. [13] on the basis of inelastic X-ray scattering in AMA $Ni_{33}Zr_{67}$, the authors relate the appearance of the low-frequency mode with longitudinal acoustic-like Ioffe–Regel excitations, the energy of which lies above the energy values of the boson peak. We note that their results contradict the models proposed for the description of acoustic properties in strong glass-forming systems [40], which predict the equality of the energy values of Ioffe–Regel excitations and the energy of the boson peak ($E_{IR} = E_{BP}$).

Recently, it was shown in Ref. [27] that the high-frequency acoustic excitations are connected with two-, three- and four-particle interactions, i.e., the main contribution to the high-frequency dynamics of the particles is produced by structural units consisting of four atoms. Taking into account that the characteristic timescale for the vibrational motions τ is inversely

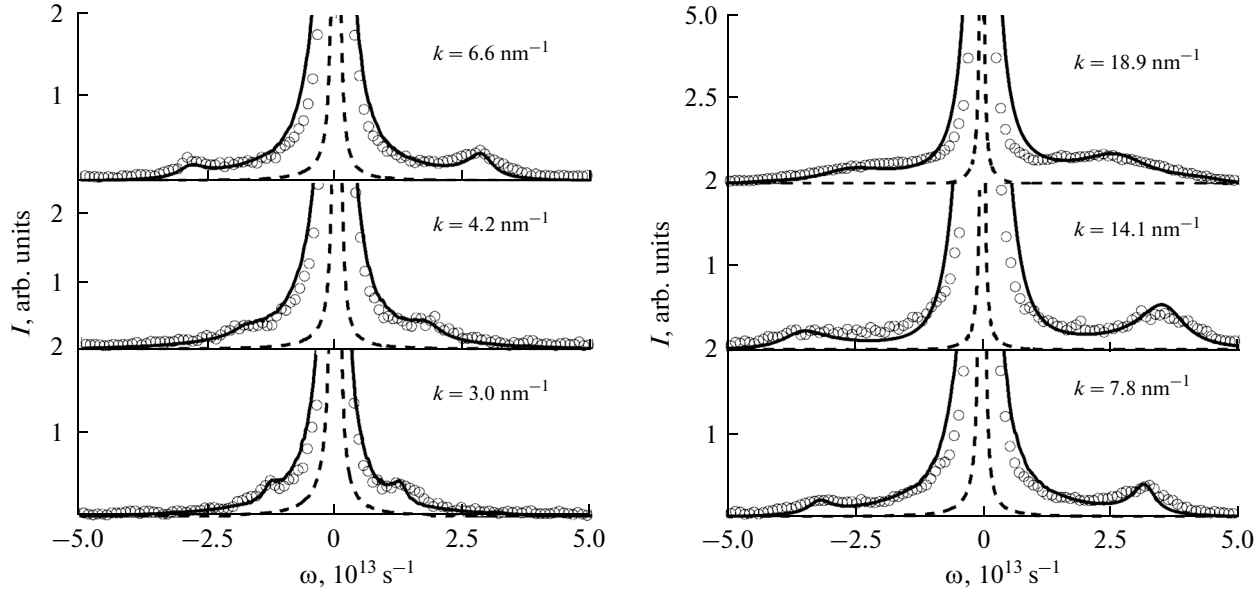

Fig. 6. Intensity of scattering for the amorphous metallic alloy $Ni_{33}Zr_{67}$ at the temperature $T = 300$ K. The solid line presents the results of the theoretical calculation (13) results corrected with the detailed balance condition (20) and the experimental resolution function (21); (○) denote experimental data on inelastic X-ray scattering [13]. The dotted line shows the experimental resolution function.

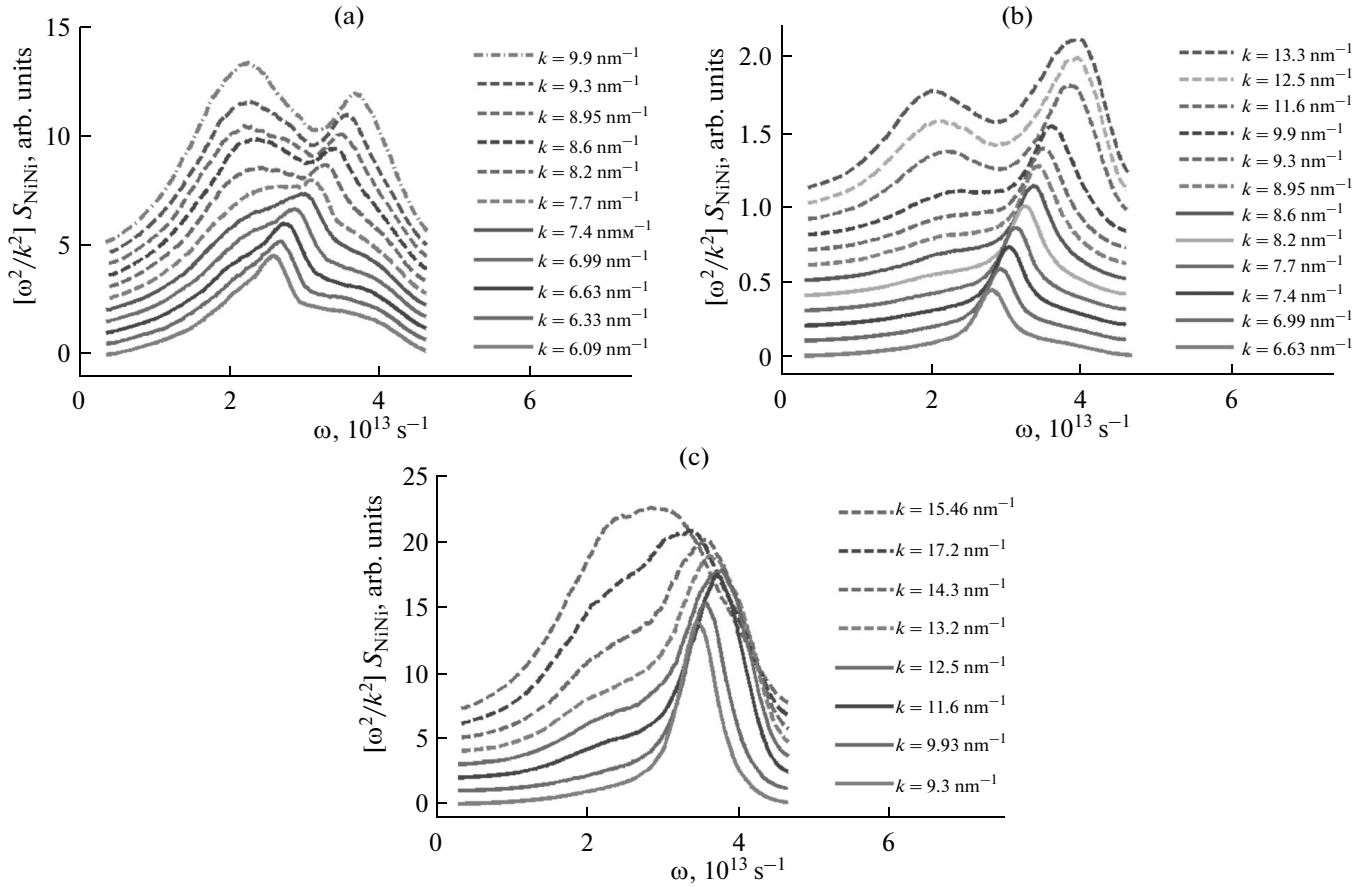

Fig. 7. Partial components of the longitudinal current spectra of $Ni_{33}Zr_{67}$ at the temperature $T = 300$ K for: (a) pairs of Ni–Ni atoms; (b) components of the Ni–Zr system and (c) Zr–Zr atoms.

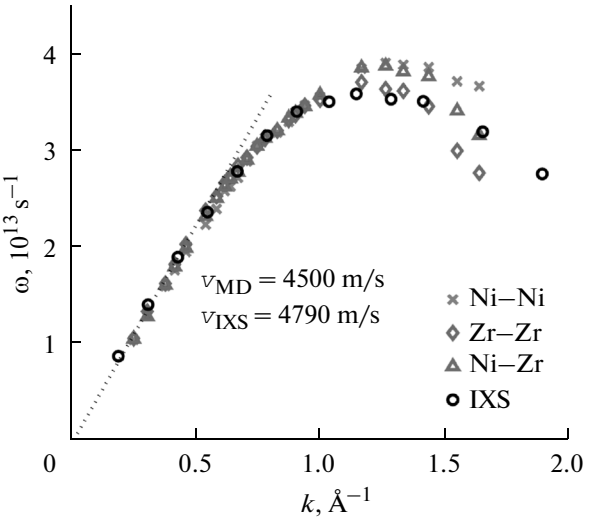

Fig. 8. Dispersion of the sound velocity for the amorphous metallic alloy $Ni_{33}Zr_{67}$ at the temperature $T = 300$ K. The dotted line shows the results of hydrodynamic theory.

proportional to the vibrational frequency ($\tau \sim 1/\omega$), we obtain that the low-frequency and high-frequency excitations are characterized, respectively, by large and small timescales [41, 42]. It can be seen from Fig. 7 that the frequency of the low-frequency excitations ($\omega_l^{\alpha,\beta}$, where $\alpha,\beta \in \{Ni, Zr\}$) in the partial components of the longitudinal current spectra is almost the same and weakly depends on the wavenumber values. Thus, it is possible to conclude that the nature of the low-frequency excitations is associated with the vibrational motion of large individual clusters (containing more than four atoms) consisting of Ni and Zr atoms.

Dispersion of the sound velocity in the system $Ni_{33}Zr_{67}$ obtained on the basis of simulations in comparison with the results of hydrodynamic theory ($\omega_c(k) = \vartheta k$) and experimental data for inelastic X-ray scattering [13] is shown in Fig. 8. It is seen from the figure that the simulation results are in a good agreement with experimental data [13], and with the asymptotic results of hydrodynamic theory. In spite of the fact that the calculated value of the sound velocity ($\vartheta_{MD} = 4500$ m/s) has a somewhat underestimated value in comparison with the experimental value $\vartheta_{MD} = 4790$ m/s), the simulation data correctly reproduce the details of the dispersion curve.

CONCLUSIONS

In this work, the MD simulation results for the bulk metallic glass $Ni_{33}Zr_{67}$ are presented. The simulation results for the structural and dynamic characteristics are in good agreement with the experimental data of neutron diffraction and inelastic X-ray scattering.

Theoretical interpretation of the simulation results was performed within the Lee's recurrent relation approach: the results of theoretical calculations of the scattering intensity spectra $I(k, \omega)$ for AMA $Ni_{33}Zr_{67}$ are in good agreement with the experimental data of inelastic X-ray scattering [13].

It was established that the low-frequency excitation observed in the longitudinal current spectra are associated with the vibrational motions of large individual clusters (including more than four atoms), consisting of Ni, and Zr atoms.

ACKNOWLEDGMENTS

We are sincerely grateful to Dr. T. Scopigno (University of Rome La Sapienza, Italy) and Professor J.-B. Suck (University of Technology Chemnitz, Germany) for sharing experimental data with us and for discussion of results.

REFERENCES

1. A. V. Mokshin and R. M. Yulmetyev, *Microscopic Dynamics of Simple Liquids* (Tsentr Innovats. Tekhnol., Kazan, 2006) [in Russian].
2. W. Clement, R. H. Willens, and P. Duwez, Nature **187**, 869 (1960).
3. A. L. Greer, Science **267**, 1947 (1995).
4. W. L. Johnson, MRS Bull. **24**, 42 (1999).
5. R. M. Khusnutdinoff and A. V. Mokshin, Bull. Russ. Acad. Sci.: Phys. **74**, 640 (2010).
6. R. M. Khusnutdinoff, A. V. Mokshin, and I. I. Khadeev, J. Phys.: Conf. Ser. **394**, 012012 (2012).
7. A. V. Mokshin, A. V. Chvanova, and R. M. Khusnutdinoff, Theor. Math. Phys. **171**, 541 (2012).
8. A. V. Nezhdanov, A. Yu. Afanaskin, A. V. Ershov, and A. I. Mashin, J. Surf. Invest.: X-ray, Synchrotron Neutron Tech. **6**, 1 (2012).
9. T. Omoto, M. Arai, Y. Inamura, J.-B. Suck, S. M. Bennington, and K. Suzuki, J. Non-Cryst. Solids **232–234**, 613 (1998).
10. W. L. Johnson, J. Matter **54**, 40 (2002).
11. Q. W. Yang and T. Zhang, J. Phys.: Condens. Matter **19**, 086212 (2007).
12. T. Omoto, M. Arai, J.-B. Suck, and S. M. Bennington, J. Non-Cryst. Solids **312–314**, 599 (2002).
13. T. Scopigno, J.-B. Suck, R. Angelini, F. Albergamo, and G. Ruocco, Phys. Rev. Lett. **96**, 135501 (2006).
14. A. A. Dyshekov, J. Surf. Invest.: X-ray, Synchrotron Neutron Tech. **4**, 956 (2010).
15. R. M. Khusnutdinov, R. M. Yulmetyev, and V. Yu. Shurygin, J. Phys.: Conf. Ser. **98**, 022010 (2008).
16. A. V. Mokshin, S. O. Zabegaev, and R. M. Khusnutdinoff, Phys. Solid State **53**, 570 (2011).
17. A. V. Mokshin, R. M. Yulmetyev, R. M. Khusnutdinoff, and P. Hänggi, J. Phys.: Condens. Matter **19**, 046209 (2007).
18. R. Yulmetyev, R. Khusnutdinoff, T. Tezel, Y. Iravul, B. Tuzel, and P. Hanggi, Phys. A **388**, 3629 (2009).
19. M. H. Lee, Phys. Rev. Lett. **51**, 1227 (1983).
20. M. H. Lee, Phys. Rev. E **62**, 1769 (2000).

21. M. H. Lee, Phys. Rev. E **61**, 3571 (2000).
22. M. H. Lee, Phys. Rev. Lett. **85**, 2422 (2000).
23. U. Balucani, M. H. Lee, and V. Tognetti, Phys. Rep. **373**, 409 (2003).
24. R. Kubo, J. Phys. Soc. Jpn. **12**, 570 (1957).
25. A. V. Mokshin, R. M. Yulmetyev, P. Hänggi, and V. Yu. Shurygin, Phys. Rev. E **64**, 057101 (2001).
26. N. N. Bogolyubov, *Problems of Dynamical Theory in Statictical Physics* (Gostekhizdat, Moscow, Leningrad, 1946) [in Russian].
27. A. V. Mokshin, R. M. Yulmetyev, R. M. Khusnutdinov, and P. Hänggi, J. Exp. Theor. Phys. **103**, 841 (2006).
28. C. Hausleitner and J. Hafner, Phys. Rev. B **42**, 5863 (1990).
29. M. P. Allen and D. J. Tildesley, *Computer Simulation of Liquids* (Clarendon, Oxford, 1987).
30. J.-P. Hansen and I. R. McDonald, *Theory of Simple Liquids* (Academic, New York, 2006).
31. A. V. Mokshin, R. M. Yulmetyev, R. M. Khusnutdinov, and P. Hänggi, Phys. Solid State **48**, 1760 (2006).
32. P. Andonov and P. Chieux, J. Phys. (Paris) **46**, C8-81 (1985).
33. D. Lee, A. Lee, C. N. J. Wagner, L. E. Tanner, and A. K. Soper, J. Phys. (Paris) **43**, C-19 (1982).
34. G. A. Korn and T. M. Korn, *Mathematical Handbook for Scientists and Engineers* (McGraw-Hill, New York, 1961).
35. A. V. Mokshin, R. M. Yulmetyev, and P. Hänggi, Phys. Rev. Lett. **95**, 200601 (2005).
36. G. Ruocco and F. Sette, J. Phys.: Condens. Matter **11**, R259 (1999).
37. S. J. Cocking and P. A. Egelstaff, J. Phys. C **1**, 507 (1968).
38. R. M. Khusnutdinov, A. V. Mokshin, and R. M. Yulmetyev, J. Exp. Theor. Phys. **108**, 417 (2009).
39. A. V. Nagornyi, V. I. Petrenko, M. V. Avdeev, L. A. Bulavin, and V. L. Aksenov, J. Surf. Invest.: X-ray, Synchrotron Neutron Tech. **4**, 976 (2010).
40. B. Ruffle, G. Guimbretiere, E. Courtens, R. Vacher, and G. Monaco, Phys. Rev. Lett. **96**, 045502 (2006).
41. R. M. Yulmetyev, A. V. Mokshin, P. Hänggi, and V. Yu. Shurygin, JETP Lett. **76**, 147 (2002).
42. A. V. Mokshin, R. M. Yulmetyev, T. Scopigno, and P. Hänggi, J. Phys.: Condens. Matter **15**, 2235 (2003).

Translated by L. Mosina